Journal of Alloys and Compounds 509 (2011) 271–275

Contents lists available at ScienceDirect

Journal of Alloys and Compounds

journal homepage: www.elsevier.com/locate/jallcom

Structure and electrical properties of $PbZrO_3$ antiferroelectric thin films doped with barium and strontium

Xihong Hao[a,b], Jiwei Zhai[a,*], Jing Zhou[c], Zhenxing Yue[d], Jichun Yang[b], Wenguang Zhao[b], Shengli An[b]

[a] Functional Materials Research Laboratory, Tongji University, Shanghai 200092, China
[b] School of Materials and Metallurgy, Inner Mongolia University of Science and Technology, Baotou 014010, China
[c] State Key Laboratory of Advanced Technology for Materials Synthesis and Processing, Wuhan University of Technology, Wuhan 430070, China
[d] State Key Laboratory of New Ceramic and Fine Processing Tsinghua University, Beijing 62772556, China

ARTICLE INFO

Article history:
Received 29 May 2010
Received in revised form 28 July 2010
Accepted 28 July 2010
Available online 4 August 2010

Keywords:
Thin film
Sol–gel processes
Microstructure
Phase transition

ABSTRACT

In this paper, we report on the structure and electrical properties of lead zirconate ($PbZrO_3$) thin films doped with barium (Ba^{2+}) and strontium (Sr^{2+}) deposited on platinum-buffered silicon substrates by a sol–gel method. Effects of Ba^{2+} and Sr^{2+} dopants on microstructure and electrical properties of the $PbZrO_3$ antiferroelectric thin films were investigated in details. X-ray diffraction patterns and scanning electron microscope micrographs illustrated that orientation and surface microstructure of these antiferroelectric films were dopant-dependent. The dielectric measurements showed that Sr^{2+} doping stabilized the antiferroelectric phase, while Ba^{2+} doping destabilized the antiferroelectric phase. It was also found that fatigue property of the antiferroelectric $PbZrO_3$ thin films was improved remarkably by the dopants.

1. Introduction

Perovskite antiferroelectric (AFE) materials usually display larger field-induced strains, higher energy storage density, considerable pyroelectric coefficient and giant electrocaloric effect due to its unique electric-field-induced phase transformation characteristics between ferroelectric (FE) and AFE. Hence, AFE materials have potential applications in micro-actuators, IR-detectors, digital memories, high energy storage capacitors and cooling devices [1–4]. Pure $PbZrO_3$ (PZ) with a Curie point of 230 °C is the most stable AFE material at room temperature [5]. PZ-based materials in bulk and film forms are also the most extensively investigated AFE materials at present. There are a lot of reports on PZ-based AFE materials, such as: (Pb,La)ZrO_3 (PLZ), (Pb,Ba)ZrO_3 (PBZ), (Pb,Sr)TiO_3 (PST), $(Pb_{0.97}La_{0.02})(Zr,Ti,Sn)O_3$ (PLZST) and $(Pb_{0.99}Nb_{0.02})(Zr,Ti,Sn)O_3$ (PNZST), and so on [6–14]. Based on these studies, it was concluded that the final properties of AFE materials either in bulk or in film forms were heavily dependent on its chemical composition. The compositionally tailored properties of AFE materials originated from the changed AFE–FE transition procedure. Although there were many studies on doped PZ AFE materials as mentioned above, almost all investigations focused on destabilizing AFE phase and the most studied ions were La^{3+} at Pb^{2+} site and Sn^{4+}, Ti^{4+} and Nb^{5+} at Zr^{4+} site. In fact, the relative stability of AFE phase could also be tailored by replacing Pb^{2+} with Ba^{2+} or Sr^{2+}, which was firstly reported by Shirane [15] in PZ ceramics. In this paper, it was found that the Curie point of AFE ceramic was decreased by Ba^{2+} doping and increased by Sr^{2+} doping. This meant that Sr^{2+} doping stabilized the AFE phase and that Ba^{2+} doping destabilized the AFE phase, as compared with pure PZ ceramic. However, it was unfortunate that electric-field-induced phase switching between AFE and FE was not available in his study because of the high threshold electric-field, which was larger than the breakdown field. It is well known that AFE films often display a higher breakdown field in contrast to bulk ceramics. Therefore, the investigation on Ba^{2+} or Sr^{2+} doped PZ AFE materials in thin film form should be more interesting. Moreover, it was reported by Wang et al. [16,17] that the fatigue property of $Pb(Zr,Ti)O_3$ thin films could be improved by Ba^{2+} or Sr^{2+} dopants. Thus, it is reasonably expected that the fatigue against endurance of PZ-based AFE thin films could also be enhanced by Ba^{2+} or Sr^{2+} doping.

In this work, 5% mole Ba^{2+} and Sr^{2+} doped PZ AFE thin films were grown on platinum-buffered substrates. Our aim was to investigate the influence of Ba^{2+} or Sr^{2+} dopants on electric-field-induced phase switching process and fatigue characteristics of the doped PZ-based AFE thin films.

2. Experimental

2.1. Synthesis

$PbZrO_3$, $(Pb_{0.95}Ba_{0.05})ZrO_3$ [PBZ(5)] and $(Pb_{0.95}Sr_{0.05})ZrO_3$ [PSZ(5)] AFE thin films were prepared by a sol–gel technique, which was similar to the reports in Refs.

* Corresponding author. Tel.: +86 21 65980544; fax: +86 21 65985179.
E-mail address: apzhai@tongji.edu.cn (J. Zhai).

0925-8388/$ – see front matter © 2010 Elsevier B.V. All rights reserved.
doi:10.1016/j.jallcom.2010.07.200

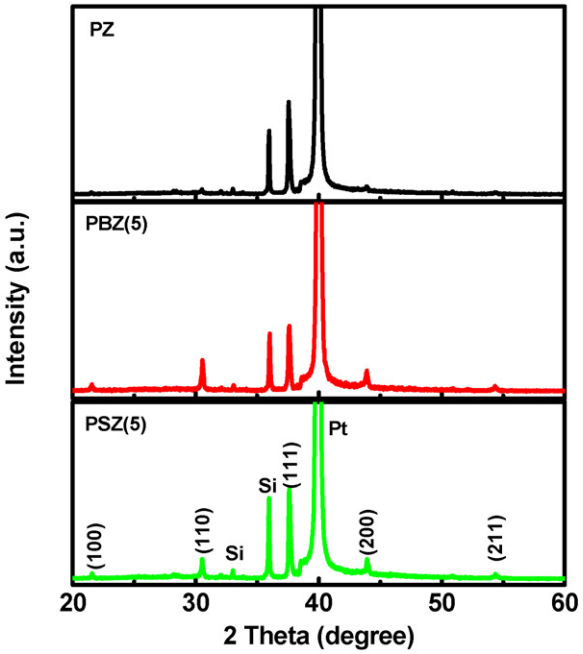

Fig. 1. XRD patterns of the PZ, PBZ(5) and PSZ(5) thin films.

[18,19]. Barium acetate (99.5%, Sinopharm Chemical Reagent Co., Ltd., China), strontium acetate (99.9%, Sinopharm Chemical Reagent Co., Ltd., China), lead acetate trihydrate (99.5%, Sinopharm Chemical Reagent Co., Ltd., China) and zirconium isopropoxide (70% in propanol, Aldrich) were used as raw materials. Glacial acetic and deionized water were used as solvents. Final concentration of the sol was 0.2 M. In order to compensate lead loss during annealing and prevent the formation of pyrochlore phase, additional ten percent of lead acetate trihydrate was added to the solution. After aged 24 h, the sol was used to deposited PZ, PBZ(5) and PSZ(5) thin films on Pt(1 1 1)-buffered silicon substrates via a multiple-spin-coating procedure. The individual layer was spin-coated at 3000 rpm for 20 s and then pyrolyzed at 450 °C for 10 min. Spin-coating and heat-treatment were repeated several times to obtain desired thickness. A capping layer was coated by using 0.4 M PbO precursor solution, which was prepared from lead acetate trihydrate, on surface of the PZ, PBZ(5) and PSZ(5) films before they were finally annealed at 700 °C for 30 min. This capping layer served the purpose of preventing excessive lead loss, thereby ensuring the formation of a single perovskite phase. Final thickness of the PZ, PBZ(5) and PSZ(5) thin films was about 500 nm.

2.2. Characterizations

Phase composition and surface microstructure of these thin films were studied by means of X-ray diffraction (XRD) patterns and scanning electron microscopy (SEM), respectively. For electrical measurements, gold pads of 0.50 mm in diameter were coated on the surface of the films by dc sputtering. Temperature and electric-field-dependent dielectric properties were analyzed using an Agilent 4284A *LCR* meter at 100 kHz. Field-induced hysteresis loops, leakage current curves and fatigue behaviors of the thin films were measured by a Radiant Technology ferroelectric tester at room temperature.

3. Results and discussion

3.1. X-ray diffractions analyses

XRD patterns of the PZ, PBZ(5) and PSZ(5) AFE thin films are shown in Fig. 1. The diffraction peaks are indexed according to pseudocubic structure rather than orthorhombic structure. As shown in Fig. 1, pure PZ film has a highly (1 1 1)-preferred orientation. Similar results were also obtained in other lead-contained AFE and FE thin films. The proposed nucleation mechanism for lead-based thin films, which were prepared by sol–gel processes on Pt(1 1 1)-buffered substrates, was attributed to the formation of a transient inter-metallic phase with (1 1 1) orientation, such as Pt_3Ti or Pt_3Pb [20]. The (1 1 1)-preferred transient inter-metallic phase served as a seed layer, which decreased activation energy for the crystallization of AFE and FE films. These films were thus induced to grow along the same (1 1 1) orientation. Clearly, although (1 1 1) peak is still the strongest one for the Ba^{2+} and Sr^{2+} doped PZ AFE thin films, (1 0 0), (1 1 0) and (2 0 0) peaks are also detected in its XRD patterns. This indicates that (1 1 1)-preferred orientation of the AFE films is degraded due to the Ba^{2+} and Sr^{2+} doping. It is probably attributed to the different ionic radius of Pb^{2+} (120 pm) from Ba^{2+} (135 pm) and Sr^{2+} (112 pm) [20,21]. The difference in ionic radius leads to an increase in crystallization energy of the films along (1 1 1) orientation. Therefore, the (1 1 1) orientation of PBZ(5) and PSZ(5) films are declined. To give a quantitative evaluation, the relationship between the (1 1 1) orientation degree $\alpha_{(1\,1\,1)}$ ($\alpha_{(111)} = I_{(111)}/(I_{(100)} + I_{(110)} + I_{(111)})$ and the difference β ($\beta = |r_{Pb} - r_{dop}|$) in ionic radius between Pb^{2+} and the dopant was investigated. β and $\alpha_{(1\,1\,1)}$ values are 8 pm and 0.75 for PSZ(5), and 15 pm and 0.62 for PBZ(5). Namely, larger β leads to smaller $\alpha_{(1\,1\,1)}$, and vice versa. Obviously, this result is consistent with the proposed mechanism.

3.2. SEM study

Fig. 2 shows typical surface microstructure images of PZ, PBZ(5) and PSZ(5) AFE thin films. All the films display a unique rosette-like characteristic, which are more uniform for the doped films. This rosette-like surface structure is typical microstructure of lead-containing films, which were also reported in PZT, PZ and PLZST films by other researchers [22–24]. It was suggested that the rosette-like structure was formed duo to the formation of Pb-rich nucleation sites along two dimensions, as well as Pb-volatilization during heat-treatment [25]. The more uniformed structure of doped PZ films further demonstrates that Ba^{2+} and Sr^{2+} doping have an obvious effect on its crystallization process. It could be predicted here that the difference of crystalline orientation and microstructure between undoped and doped PZ thin films certainly have some influence on its final dielectric properties.

3.3. Dielectric properties

Fig. 3 illustrates electric-field-dependent dielectric constant (ε_r–E) and loss tangent ($\tan\delta$) of the PZ, PBZ(5) and PSZ(5) AFE thin films. The measurements were carried out at room temperature and at frequency of 100 kHz. The *dc* voltage was stepped through 0.5 V increments with a time lag of 0.5 s. Both dielectric constant and dielectric loss of the films display a double-butterfly shape, corresponding to the transformation between AFE to FE phase and confirming AFE nature of films. Dielectric constant increases sharply at the moment of AFE–FE transition, and then drops when the curve saturated. The variation of dielectric constant at the FE–AFE switching also displays a similar tendency, but the increase in dielectric constant is slightly smaller than that in the case of AFE–FE transition. The magnitude of phase switching fields could be determined from the peaks of ε_r–E curves. The forward switching fields E_F are 350, 250 and 440 kV/cm, and the reverse switching fields E_{AF} are 260, 130 and 420 kV/cm for the PZ, PBZ(5) and PSZ(5) thin films, respectively. As compared to pure PZ AFE films, the decreased switching fields for the PBZ(5) films illustrate that AFE phase is destabilized by Ba^{2+} doping, and the increased transition fields for the PSZ(5) demonstrate that AFE state is stabilized by Sr^{2+} doping. According to [26,27], the Goldsmith tolerance factor describes the stability of the perovskite structure (ABO_3) and is defined as:

$$t = \frac{r_A + r_O}{\sqrt{2}(r_B + r_O)},$$

where r_A, r_B, and r_O are the ionic radii of A-site cation, B-site cation, and oxygen anion, respectively. It is believed that films are in AFE

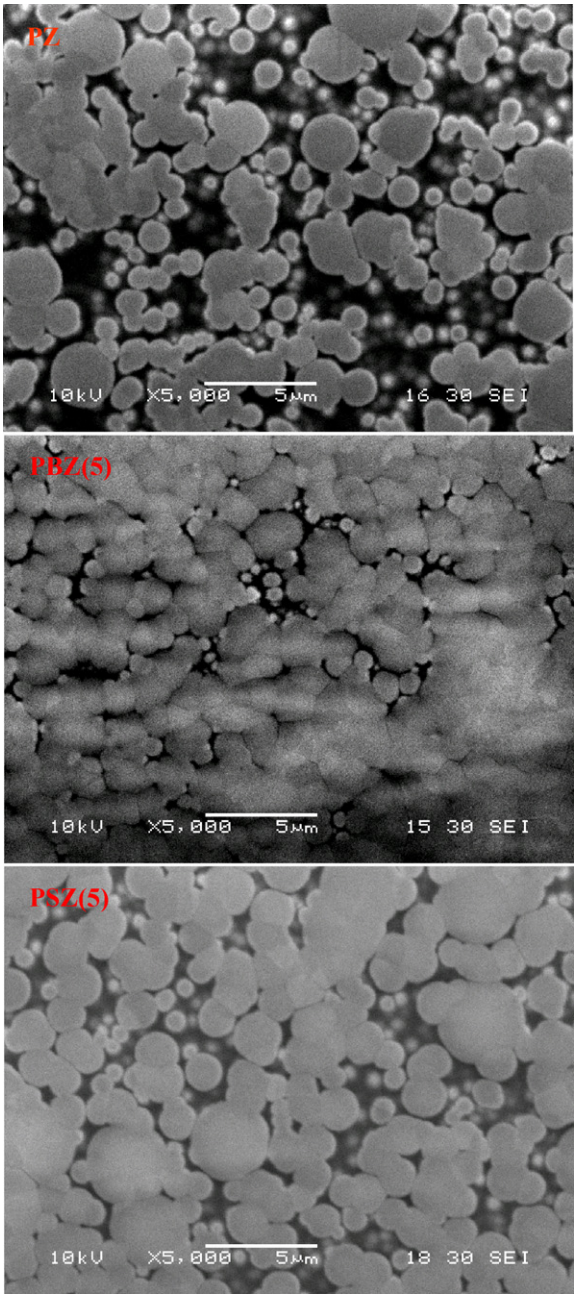

Fig. 2. SEM images of the PZ, PBZ(5) and PSZ(5) thin films.

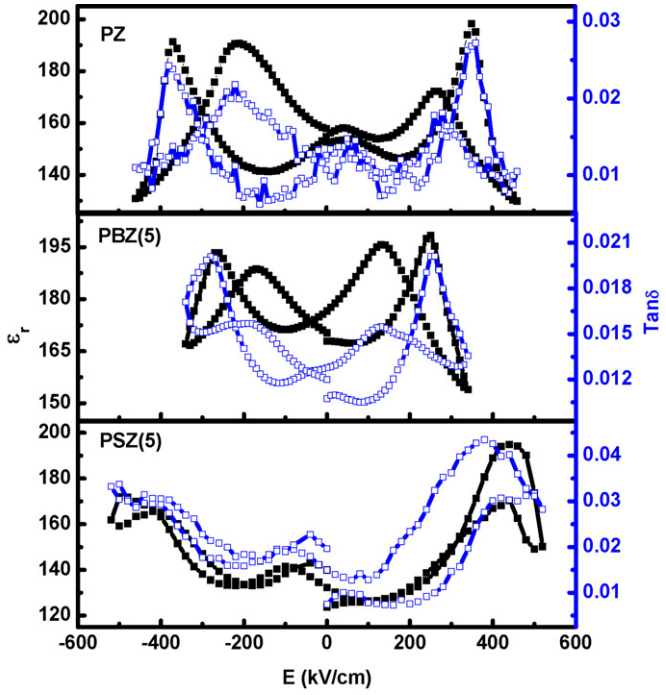

Fig. 3. Electric-field dependence of dielectric constant (closed square) and dielectric loss (open square) of the PZ, PBZ(5) and PSZ(5) thin films measured at 100 kHz.

state for $t < 1$. Thus, the phase transition behaviors of PZ-based AFE materials could be controlled by doping proper ions at A or/and B site. In our present work, the ions radius of Ba^{2+} is larger, and the ions radius of Sr^{2+} is smaller than that of Pb^{2+}. Consequently, the t value is increased in the Ba^{2+}-doped case and decreased in the Sr^{2+}-doped case, respectively. Therefore, AFE phase is stabilized for PSZ(5) and is destabilized for PBZ(5).

Polarization–field (*P*–*E*) loops of these AFE films are shown in Fig. 4, which were measured at 1 kHz and at room temperature. The double hysteresis loops further demonstrate AFE nature of the PZ, PBZ(5) and PSZ(5) films. However, as compared to PZ and PSZ(5), a smaller remnant polarization is observed for PBZ(5). This result indicates that Ba^{2+} doping leads to the appearance of FE phase in the film. Transformation thresholds between AFE and FE phase could also be estimated by extrapolating the two steepest sections of the hysteresis loops and obtaining its intersections with horizontal axis. Accordingly, E_F values are 450, 280 and 500 kV/cm, and E_{AF} values are 260, 110 and 330 kV/cm for the PZ, PBZ(5) and PSZ(5), respectively. It shows the same tendency with the corresponding values obtained from ε_r–*E* curves. However, the values obtained from *P*–*E* and ε_r–*E* measurements are different. This difference may be resulted from the different measurement methods. *P*–*E* curves were measured with a triangle wave, while ε_r–*E* curves were measured with a *dc* bias plus a weak *ac* wave.

Temperature dependence of dielectric constant of the AFE thin films are plotted in Fig. 5(a), which were measured at 100 kHz. With increasing temperature, dielectric constant gradually increases to maximum value (ε_m) at Curie temperature (T_c), and then decreases smoothly. T_c obtained from Fig. 5(a) is 494, 462 and 521 K for PZ, PBZ(5) and PSZ(5), respectively. This result is consistent with Shirane's observation. It is well known that antiferroelectrics above Curie temperature, similar to ferroelectrics, also fellow the

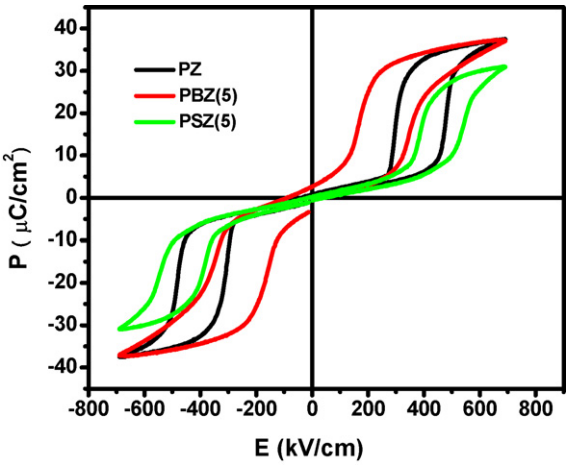

Fig. 4. Hysteresis loops of the PZ, PBZ(5) and PSZ(5) thin films measured at 1 kHz.

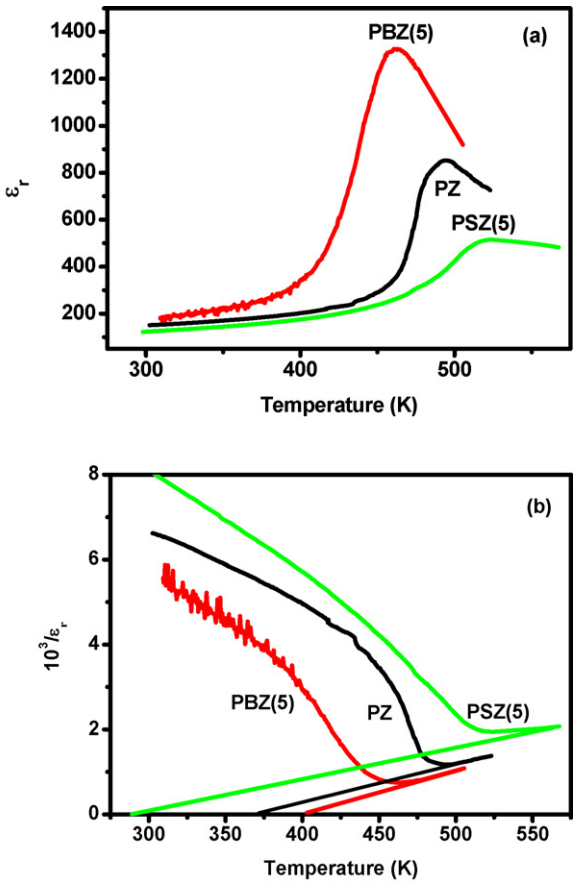

Fig. 5. Temperature-dependent dielectric constant of the PZ, PBZ(5) and PSZ(5) thin films measured at 100 kHz (a), and their inverse dielectric constant as a function of temperature (b).

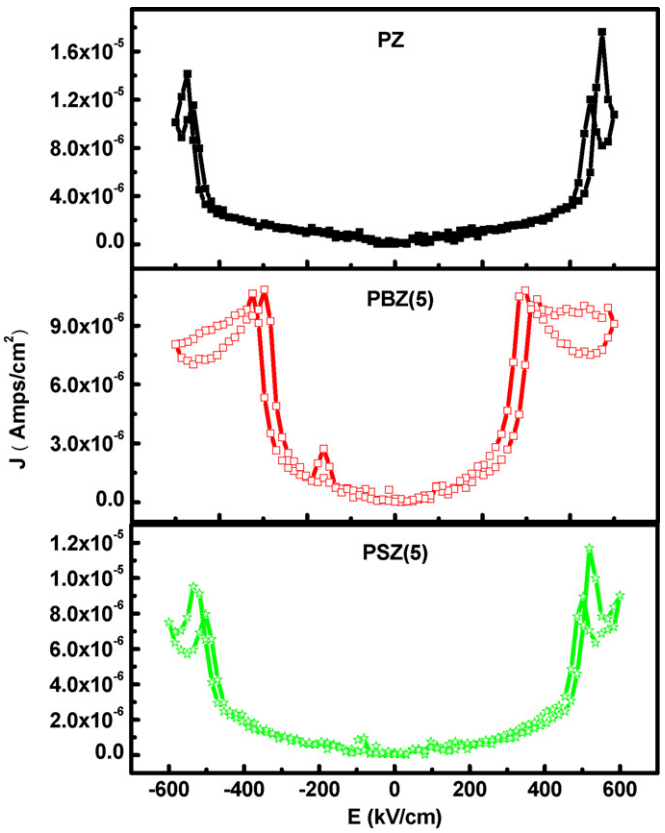

Fig. 6. Electric-field-dependent current of PZ, PBZ(5) and PSZ(5) thin films.

Curie–Weiss law [27]:

$$\frac{1}{\varepsilon} = \frac{T - T_0}{C} \quad (T > T_0)$$

where T_0 is the Curie–Weiss temperature and C is the Curie–Weiss constant. Inverse dielectric constant as a function of temperature is plotted in Fig. 5(b), where the experimental data are fitted by using a nonlinear curve-fitting program, according to above equation. Clearly, the temperature-dependent dielectric constant of all films are well obeyed the Curie–Weiss law above Curie temperature. Following the internal field model of dielectrics at higher temperature, the degree of ferroelectric coupling between local dipoles could be related to the Lorentz polarization factor γ, which was defined as $\gamma = T_0/C$ [24]. The calculated γ value from the fitting parameters is 3.5×10^{-3}, 2.1×10^{-3} and 4.1×10^{-3} K for PZ, PSZ(5) and PBZ(5), respectively. Namely, γ value is decreased by Sr^{2+} doping and increased by Ba^{2+} doping. This indicates that the long-range FE coupling between diploes is weakened by Sr^{2+} substitution and that the short range AFE coupling is enhanced. While the substitution of Ba^{2+} strengthens the long-range FE coupling and decreases the short range AFE coupling.

3.4. J–E curves analyses

Fig. 6 illustrates electric-field-induced current (J–E) curves of all AFE thin films. The time delay between the change of voltage and the acquisition of data was 100 ms. It should be noted that the measured current includes leakage current and polarization-induced current caused by the turning of dipole during polarization and depolarization process. Because of the excellent quality of our films and the smaller time delay of measurements, leakage current is very small and polarization-induced current is dominant in the measured current. As shown in Fig. 6, four obvious current peaks, which have the largest current values at the order of 10^{-5} A/cm^2 for all the films, illustrate a considerable current produced during phase transformation between AFE and FE phase. During polarization process, electric-field has the same direction with leakage current and phase switching current. Therefore, maximum current value is observed in this process. The maximum current density is 1.8×10^{-5} A/cm^2 at 475 kV/cm^2, 1.1×10^{-5} A/cm^2 at 323 kV/cm^2 and 1.2×10^{-5} A/cm^2 at 510 kV/cm^2, for PZ, PBZ(5) and PSZ(5), respectively. The difference in maximum current density is related to phase switching speed and amount of the polar per area. During depolarization process, electric-field and leakage current are in the same direction, which are opposite to the current induced by the phase transformation from FE to AFE. As a result, the measured current for FE–AFE is smaller than that for AFE–FE.

3.5. Fatigue characteristics

Polarization fatigue (PF) behaviors of the AFE thin films were also investigated at room temperature, as depicted in Fig. 7. The fatigue experiment was performed using a sine pulse at 10 kHz and at the maximum external electric field of 600 kV/cm. P_N denotes the values of saturation polarization (P^*) after N-switching cycles. As shown in Fig. 7, the reduction of P_N after 10^8 switching is 49% 12% and 28%, for the PZ, PBZ(5) and PSZ(5) thin films, respectively. This indicates that Ba^{2+} and Sr^{2+} doping significantly improve the fatigue resistance of AFE thin films. This result is similar to the PF behavior of Ba^{2+}- and Sr^{2+}-doped $Pb(Zr_{0.52}Ti_{0.48})O_3$ thin films [13,14]. It was concluded that the enhanced PF endurance of doped PZ films was contributed to the decrease of oxygen vacancy density and the suppression of mobility by Ba^{2+} and Sr^{2+} doping. The

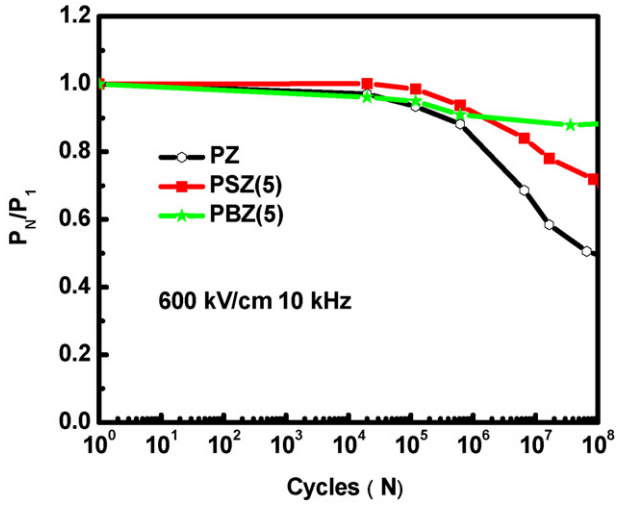

Fig. 7. Polarization fatigue properties of the PZ, PBZ(5) and PSZ(5) thin films measured at 600 kV/cm.

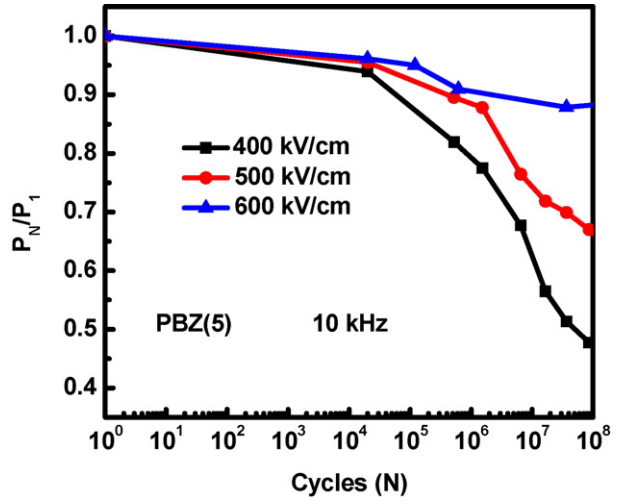

Fig. 8. Polarization fatigue properties of the PBZ(5) films measured at 400, 500 and 600 kV/cm, respectively.

decrease of oxygen vacancy density and its suppressed mobility were ascribed to the stronger bonding energy of the Sr–O bond (426 kJ/mol) and the Ba–O bond (562 kJ/mol) than that of the Pb–O bond (382 kJ/mol). Because of the stronger bonding energy of Ba–O than that of Sr–O, Ba^{2+}-doped PZ AFE thin films show the best fatigue against performance.

Fig. 8 shows PF properties of the PBZ(5) thin films at different external fields of 400, 500 and 600 kV/cm. It is evident that high external electric-field is favor to the improvement of fatigue endurance. According to the fatigue mechanism proposed by Wang et al. [28], the appearance of fatigue generally originates from following two aspects. One is long-range diffusion of defects, such as: oxygen vacancy, at external electric-field. The other is domain wall pinning under repeated switching of domains. When domain wall pinning is dominant, films would display better fatigue against performance at high fields. This is because larger electric-field makes the domain switching and depinning easier. Therefore, domain wall pinning is the main resource of the fatigue emergence in our AFE films.

4. Conclusions

In summary, substitution of Ba^{2+} and Sr^{2+} had a significant influence on the growth behavior and electrical performance of PZ-based AFE thin films. Compared to pure PZ AFE thin films, PBZ(5) and PSZ(S) displayed a uniform microstructure with a decreased (1 1 1) orientation. AFE phase was stabilized by Sr^{2+} doping and destabilized by Ba^{2+} doping, which could be explained by the variation of the tolerance t. Because of the higher bonding energy of Sr–O and Ba–O than that of Pb–O, the fatigue endurance of doped AFE films was improved greatly. The fatigue measurement results under different maximum external electric-field demonstrated that the domain wall pinning was the main resource of fatigue emergence in our AFE films.

Acknowledgements

The authors would like to acknowledge the financial support from the National Natural Science Foundation of China, the Key Project of Chinese Ministry of Education under grant No.210038, the Chunhui Plan of Chinese Ministry of Education under grant No. Z2009-1-01036, the Research Fund for Higher Education of Inner Mongolia under grant No. NJ09080, the project of State Key Laboratory of Advanced Technology for Materials Synthesis and Processing (Wuhan University of Technology) under grant No. 2010-KF-5, and the project of State Key Laboratory of New Ceramic and Fine Processing Tsinghua University.

References

[1] S.E. Park, K. Markowski, S. Yoshikawa, L.E. Cross, J. Am. Ceram. Soc. 80 (1997) 407.
[2] J. Parui, S.B. Krupanidhi, J. Appl. Phys. 100 (2006) 044102.
[3] Z.K. Xu, J.W. Zhai, W.H. Chan, Appl. Phys. Lett. 88 (2006) 132908.
[4] G.R. Love, J. Am. Ceram. Soc. 73 (1990) 323.
[5] S. Chattopadhyay, P. Ayyub, V.R. Palkar, M.S. Multani, S.P. Pai, S.C. Purandare, R. Pinto, J. Appl. Phys. 83 (1998) 7808.
[6] S.S.N. Bharahwaja, S.B. Krupanidhi, Thin Solid Films 423 (2003) 88.
[7] B.M. Xu, Y.H. Ye, L.E. Cross, J. Appl. Phys. 87 (2000) 2507.
[8] J.W. Zhai, M.H. Cheung, Z.K. Xu, X. Li, Appl. Phys. Lett. 81 (2002) 3621.
[9] H.W. Chen, C.R. Yang, J.H. Zhang, Y.F. Pei, Z. Zhao, J. Alloys Compd. 486 (2009) 615.
[10] X.H. Hao, J.W. Zhai, J. Cryst. Growth 310 (2008) 1137.
[11] X.H. Hao, J.W. Zhai, X. Yao, J. Cryst. Growth 311 (2008) 90.
[12] L.B. Kong, J. Ma, W. Zhu, O.K. Tan, J. Alloys Compd. 322 (2001) 290–297.
[13] P. Charoonsuk, S. Wirunchit, R. Muanghlua, S. Niemcharoen, B. Boonchom, N. Vittayakorn, J. Alloys Compd. (2010), doi:10.1016/j.jallcom.2010.06.197.
[14] X.H. Hao, Z.Q. Zhang, J. Zhou, S.L. An, J.W. Zhai, J. Alloys Compd. 501 (2010) 358–361.
[15] G. Shirane, Phys. Rev. 86 (1952) 219.
[16] Y. Wang, Q.Y. Shao, J.M. Liu, Appl. Phys. Lett. 88 (2006) 122902.
[17] Y. Wang, K.F. Wang, C. Zhu, T. Wei, J.S. Zhu, J.M. Liu, J. Appl. Phys. 101 (2007) 046104.
[18] J.W. Zhai, Y. Yao, X. Li, T.F. Hung, Z.K. Xu, H. Chen, E.V. Colla, T.B. Wu, J. Appl. Phys. 92 (2002) 3990.
[19] X.H. Hao, J.W. Zhai, X. Yao, J. Am. Ceram. Soc. 92 (2009) 286.
[20] R.D. Shannon, Acta Crystallogr. A 32 (1976) 751.
[21] S.H. Leal, J.C. Sczancoski, L.S. Cavalcante, M.T. Escote, J.M.E. Matos, M.R.M.C. Santos, F.M. Pontes, E. Longo, J.A. Varela, J. Sol–Gel Sci. Technol. 53 (2010) 21.
[22] X.G. Tang, J. Wang, X.X. Wang, H.L.W. Chan, Solid State Commun. 130 (2004) 373.
[23] X.H. Hao, J.W. Zhai, J. Phys. D: Appl. Phys. 40 (2007) 7447.
[24] L. Pintilie, I. Boerasu, M.J.M. Gomes, M. Pereira, Thin Solid Films 458 (2004) 114.
[25] E.M. Alkoy, S. Alkoy, T. Shiosaki, Jpn. J. Appl. Phys. 44 (2005) 6654.
[26] M. Johnsson, P. Lemmens, in: H. Kronmüller (Ed.), Handbook of Magnetism and Advanced Magnetic Media, John Wiley & Sons, New York, 2006, cond-mat/0506606.
[27] W.H. Chan, Z. Xu, T.F. Hung, H. Chen, J. Appl. Phys. 96 (2004) 6606.
[28] Y. Wang, K.F. Wang, C. Zhu, J.M. Liu, J. Appl. Phys. 99 (2006) 044109.